

Complexation of calix[4]arene protected gold nanoparticles with pyridinium and bipyridinium compounds

Cite this: *RSC Advances*, 2013, 3, 733

Petri M. S. Pulkkinen, Szymon Wiktorowicz, Vladimir Aseyev and Heikki Tenhu*

Calix[4]arene and calix[4]arene/alkanethiol protected gold nanoparticles with narrow size distributions were synthesised and characterized with NMR, thermogravimetric analysis (TGA) and a transmission electron microscope (TEM). NMR and light scattering (LS) were used to study the complexation of the nanoparticles with a pyridinium modified polyethylene oxide (Pyr-PEO_{2k}-Pyr) complexant and a small 16 carbon pyridinium compound (Pyr-C16). Results give clear evidence of complexation induced aggregation of the nanoparticles as pyridinium proton signals shift upon changing the host : guest ratio and LS shows a change from a narrow size distribution into a broad one. The addition of alkanethiols with longer dimensions than that of the calixarene derivative and the type of the complexant can be used to tune the complexation. The studies also provide evidence of induced fit complexation into calix[4]arene cavities and solution phase interdigitation (secondary monolayer formation) when the nanoparticles are complexed with Pyr-C16.

Received 19th June 2012,
Accepted 3rd November 2012

DOI: 10.1039/c2ra21761a

www.rsc.org/advances

Introduction

Nanoscale gold atom clusters, gold nanoparticles, have gained steadfast interest from the scientific community since original work of Brust *et al.* in the nineties.¹ Gold nanoparticles can be regarded as fascinating nanotechnological objects with many optical, electrical and catalytic properties that are tuneable with the size of the particles due to the quantum size effect.²

Calixarenes are cyclic basket-like compounds known to be important in supramolecular chemistry, mainly due to their ability to engage in the guest–host interactions.³ The properties of calixarenes can be tuned by modification of the upper and the lower rim, this offers a wide range of interesting functionalities and possible applications.

In the past, gold nanoparticles have been complexed with numerous different compounds, such as DNA and cyclodextrin, to name just a few.⁴ Calix[4]arene protected nanoparticles are of particular interest for nanotechnology applications due to the fact that calix[4]arenes are among the smallest known basket-like organic compounds with a complexation ability.

Although gold nanoparticles and calixarenes have been known for decades, increased interest towards the scientific field of calixarene-modified gold nanoparticles has surfaced relatively recently,⁵ the main interest focusing on various catalysis,⁶ sensor⁷ or molecular recognition⁸ systems. In an UV-visible spectrometry study, Ciesa *et al.* observed aggregation of such nanoparticles *via* small organic ligands.⁹ Dionisio

et al. employed a well known¹⁰ NMR ppm shift method to establish the guest–host interactions between nanoparticles carrying disulfide modified tetraphosphonate cavitands and pyridinium modified short polyethylene oxide polymers.¹¹ Ha *et al.* have also worked extensively with calixarene nanoparticles.^{6,12–14}

The development of future nanotechnological devices *via* bottom-up methodology is dependent on the targeting of nano-sized active components to the required location in the device.² Nanoparticles inheriting the guest–host interactions of the cavitands attached to their surface may reveal answers to such problems in the future.

The aim of this study is to examine the aggregation behavior of calixarene derivatized gold nanoparticles with pyridinium compounds using proton NMR and light scattering methods. A combination of such methods has not been used in the literature to quantitatively link the complexation of the metal surface bound calixarene with the aggregation behavior of the nanoparticles. The NMR methodology provides important information about the mechanism of the complexation, while light scattering allows the observation and characterization of the formed aggregates. Knowledge of the complexation behavior is expanded by experimentation with a polymeric complexant carrying pyridinium moieties on both ends. The behavior with a small organic compound carrying a single pyridinium group is also examined. Finally, a novel method of fine-tuning the complexation with addition of alkanethiols with varying aliphatic tail lengths is presented.

Laboratory of Polymer Chemistry, Department of Chemistry, University of Helsinki, P.O.Box 55, 00014 Helsinki, Finland. E-mail: heikki.tenhu@helsinki.fi

Experimental

Materials and methods. Cetyl pyridinium chloride (Pyr-C16) and other chemicals were purchased from Aldrich and Fluka. Solvents were distilled and reactants dried in a vacuum desiccator prior use. The starting materials *t*-butyl calixarene¹⁵ and 1-tosyloxyundec-10-ene¹⁶ were synthesised as described elsewhere.

The synthesis of Pyr-PEO2k-Pyr was adapted and combined from multiple references^{16,17} and is shown in Fig. 1.

In all synthesis phases, thorough vacuum drying was performed for the hygroscopic PEO2k (polyethylene oxide, MW 2000) polymer or its derivatives. 1 eq. PEO2k was mixed under a N₂ atmosphere at room temperature with 20 eq. 4-toluenesulfonyl chloride and 40 eq. triethylamine in dichloromethane (50 ml per eq. of PEO2k). The mixture was stirred for 3 days and the product was purified by precipitation from THF into diethyl ether. Further purification was performed by passing the product through a long plug of silica (75 : 25 CH₂Cl₂ : cyclohexane) and dried. Yield: 60%. 1 eq. of the tosylated PEO2k was dissolved in DMF (15 ml per eq. of tosylated PEO2k) with 8 eq. of NaBr. The mixture was stirred at 40 °C for 24 h. The polymer was purified by precipitation from THF into cold ether. Yield: 75%. Finally, 1 eq. of the brominated PEO2k was mixed with 15 eq. of pyridine in acetonitrile (30 ml per eq. of brominated PEO2k) and refluxed for two days. The product was precipitated from MeOH into cold ether and twice from MeOH into hexane. Yield: 90%. NMR and elemental analysis both indicated 90% pyridinium terminal group substitution. MALDI-TOF analysis indicated a *M_n* difference of 169 g mol⁻¹ between the starting PEO2k and the product Pyr-PEO2k-Pyr, matching the molar masses of two pyridinium groups. The polymer polydispersity, 1.03, remained unchanged. ¹H NMR (500 MHz, CDCl₃) δ 9.59 (4H, d), 8.56 (2H, t), 8.12 (4H, t), 5.27 (4H, t), 4.10 (4H, t), 3.70–3.50 (180H, m).

The calixarene lower rim modification procedure is shown in Fig. 2.

Synthesis of Calix0. 1 eq. *t*-butyl calixarene was mixed with 6 eq. of phenol and 8 eq. of AlCl₃ in 15 ml of toluene per eq. of *t*-butyl calixarene under a nitrogen flow. The reaction was run overnight at 60 °C. The resulting mixture was cooled to room

temperature and poured into 3% HCl (30 ml per eq. of *t*-butyl calixarene) and stirred for 30 min. The organic part was extracted with water and dried over Na₂SO₄. The crude product was dried and MeOH was added. The precipitate was collected by filtration. The purity was improved by recrystallization from a chloroform/MeOH mixture. Typical yield was around ~70%. ¹H NMR (500 MHz, CDCl₃) δ 10.23 (4H, s), 7.08 (8H, d), 6.76 (4H, t), 4.30 (4H, broad), 3.57 (4H, broad).

Synthesis of Calix1 was conducted by modifying an existing literature method.¹⁶ 1 eq. of Calix0 was mixed with 10 eq. of K₂CO₃ in acetonitrile (15 ml per eq. of starting calixarene). 2 eq. of 1-tosyloxyundec-10-ene was added after stirring the mixture for 1 h at room temperature. The reaction was run for 3 days under reflux conditions. The reaction mixture was dried in a vacuum, dissolved in dichloromethane and then extracted with 1 M HCl and water. The product was dried with Na₂SO₄ and evaporated to dryness. The crude product was purified using column chromatography (SiO₂, CH₂Cl₂ : cyclohexane 75 : 25, *R_f* 75%). Yield was typically ~50%. NMR showed full substitution of the two aromatic hydroxyl groups per calixarene. ¹H NMR (300 MHz, CDCl₃) δ 8.25 (2H, s), 7.07 (4H, d), 6.93 (4H, d), 6.80–6.63 (4H, m), 5.82 (2H, quin.), 4.98 (2H, d), 4.33 (4H, d), 4.01 (4H, t), 3.38 (4H, d), 2.07 (8H, m), 1.71 (8H, m), 1.5–1.3 (24H, m).

Synthesis of Calix2 was conducted by following an existing literature method.⁸ Briefly, 1 eq. of Calix1 and 4 eq. of thioacetic acid were dissolved in toluene (25 ml per eq. of Calix1) under an argon flow. After 30 min of argon bubbling, a catalytic amount of AIBN was added and the mixture was refluxed overnight. Solvent was evaporated and the crude product was dissolved in CH₂Cl₂ and extracted with a concentrated NaHCO₃ solution and water, and then dried over Na₂SO₄. The product was thoroughly dried and dispersed in ethanol (poor solubility, 15 ml per eq. Calix1). Concentrated MeOH/MeONa solution was added under vigorous stirring and the mixture was further stirred at room temperature for 24 h. Solvent was evaporated, the solid residue was dissolved in CH₂Cl₂ and extracted with 2 M HCl and water. After Na₂SO₄ drying and thorough drying in a vacuum, the product was recrystallized from a chloroform/MeOH mixture. Common reaction yields were ~60%. NMR data showed full disappearance of the double bond signals. Integration indicated full

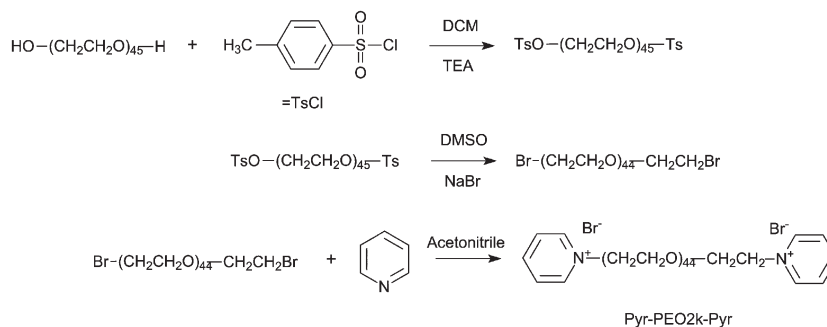


Fig. 1 The reaction pathway to Pyr-PEO2k-Pyr.

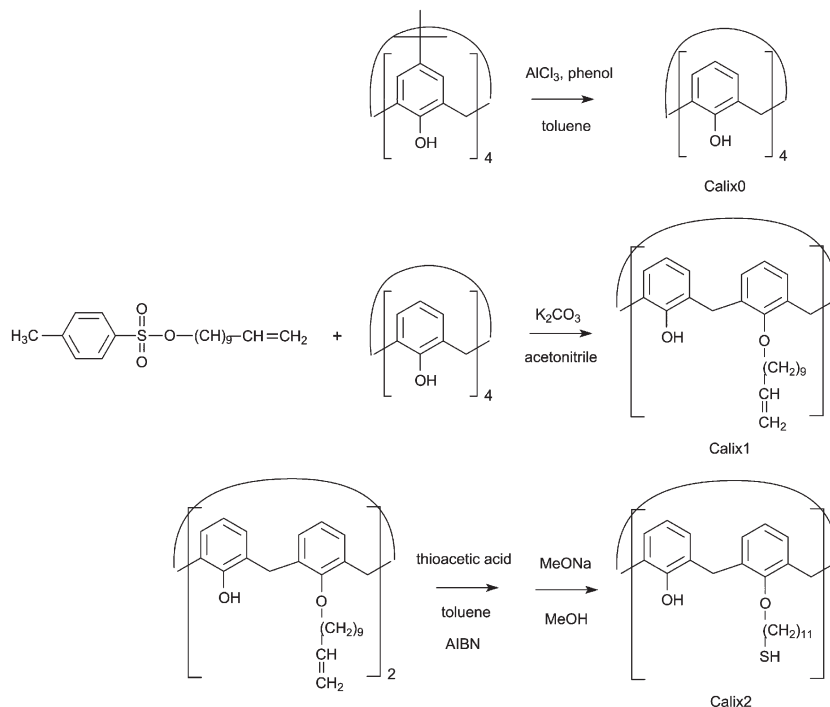


Fig. 2 The reaction pathway to thiol modified calix[4]arene.

addition of the SH groups into the double bonds. $^1\text{H NMR}$ (500 MHz, CDCl_3) δ 8.24 (2H, s), 7.06 (4H, d), 6.93 (4H, d), 6.80–6.63 (4H, m), 4.34 (4H, d), 4.01 (4H, t), 3.39 (4H, d), 4.01 (4H, t), 2.70 (4H, m), 2.07 (4H, m), 1.71–1.28 (28H, m).

Synthesis of AuNPs (reaction shown in Fig. 3) was conducted as described in the literature.¹⁸ The synthesis was conducted with 300 mg (0.88 mmol) of $\text{HAuCl}_4 \times 3\text{H}_2\text{O}$. Briefly, 3.5 eq. of tetraoctylammoniumbromide (TOAB) was dissolved in toluene (90 ml per eq. of HAuCl_4). 1 eq. of HAuCl_4 in water (20 ml per eq. of HAuCl_4) was added and the mixture was stirred vigorously. After all the gold was transferred to toluene, 14 eq. of NaBH_4 in water (20 ml per eq. of HAuCl_4)

was added as a single fast injection into the vigorously stirred mixture. The mixture was stirred for 2 h, after which the toluene phase was extracted with 0.1 M H_2SO_4 , 1 M Na_2CO_3 and water. The toluene phase was dried with Na_2SO_4 and filtered.

0.6 eq. per HAuCl_4 of Calix2 was added and the mixture was stirred for one week at room temperature in order to obtain maximal ligand exchange from TOAB into the thiol modified calixarene. In order to obtain gold nanoparticles with calixarene, calixarene/butanethiol and calixarene/dodecanethiol protection, the resulting mixture was divided into three flasks. Butanethiol or dodecanethiol were added (1 eq. per HAuCl_4 present in the flask) to the corresponding flasks and stirred for 1 h at room temperature. All the samples containing gold nanoparticles protected by calixarene, calixarene/butanethiol and calixarene/dodecanethiol ligands were purified through the same method presented here. NPs were precipitated by addition of ethanol and filtered onto a glass filtration frit. Copious amounts of ethanol and acetone were poured through the filter. Particles were collected from the frit with chloroform and purified and fractionated using a centrifuge. Methanol was added to the nanoparticles dispersed in chloroform (40 : 60 MeOH : chloroform) and centrifugation at 3773 relative centrifugal force (RCF) for 15 min precipitated the particles. The supernatant was removed, the precipitate was again dissolved in chloroform and centrifugation at 340 RCF for 10 min was performed. The small precipitate consisting of larger gold particles and aggregates was discarded and the supernatant was mixed with methanol. Centrifugation at 8720 RCF for 20 min precipitated the particles of the desired size

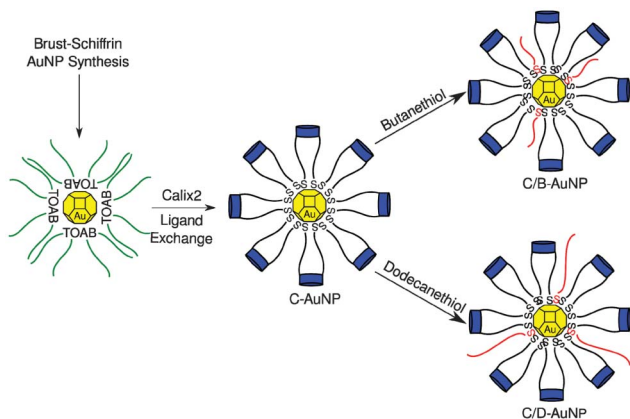


Fig. 3 The synthetic pathway to calixarene (C-AuNP), calixarene/butanethiol (C/B-AuNP) and calixarene/dodecanethiol (C/D-AuNP) protected nanoparticles.

range, which were collected. The particles were analyzed by NMR and were observed to be spectroscopically pure (Fig. 4). After purification, the gold yield was around 50%.

Characterization

UV-vis measurements were performed using a Shimadzu UV-1601PC spectrometer with quartz cuvettes. Samples were diluted until a satisfactory absorption intensity (absorbance ~ 0.5) was obtained.

Thermogravimetry (TGA) measurements were done under a flowing nitrogen atmosphere using Mettler-Toledo TGA850 equipment with STARe software. The temperature range was 25–800 °C and a heating rate of 10 °C min⁻¹ was used. TGA results were used to estimate the amount of calixarene on the particles. This data was used to calculate the calixarene and complexant amounts to be used in the NMR studies.

For transmission electron microscopy (TEM), diluted dispersions of nanoparticles (~ 1 mg ml⁻¹) were dried onto a holey carbon grid, copper mesh TEM grids, which were then observed using bright-field TEM on a FEI Tecnai 12 transmission electron microscope. Images were analyzed with the ImageJ software. Over one thousand nanoparticles per sample were included in the size distribution determination.

NMR studies for reaction products were performed either on a Bruker 500 MHz or a Varian 300 MHz NMR system. The mixed monolayers were detached from the gold nanoparticle surface by using the iodine death reaction.^{19,20} Iodine was added to the NMR tube containing the nanoparticles and the tube was shaken for several minutes. After allowing the tube to stand for a few hours, the NMR spectrum was recorded and it was observed that the broad signals from the nanoparticle bound ligands were replaced with sharp signals originating from the free ligands. The complexation experiments were performed on the higher resolution Bruker 500 MHz system. All proton spectra measurements were done in deuterated chloroform, 100 pulses, 5 s relaxation delays. Using the TGA

studies, the amount of calixarene per each nanoparticle was determined. An accurately weighted amount of nanoparticles were dispersed into 1 ml of deuterated chloroform. A concentrated solution of the complexant was prepared separately by accurately measuring a known amount of the substance and dissolving it into a known volume of deuterated chloroform. The amount of the complexant solution required to achieve a desired calixarene : complexant ratio was calculated using the TGA data. A required amount of the complexant solution was added into the gold nanoparticle NMR sample tube using a micropipette. The tube was shaken for a few minutes to mix the contents. After measuring the NMR spectrum for one ratio, another calculated dose of the complexant solution was added to the same NMR tube. This cycle was repeated until the NMR spectra were recorded for all calixarene : complexant ratios ranging from 6.0 to 0.25. The NMR spectra of the aromatic areas of pyridinium and calixarene were of particular interest, because these signals are known to shift their positions upon complexation, *i.e.*, alterations in their electronic environment.

For the estimation of the dimensions of the compounds, computational visualization was performed using Accelrys Material Studio 4.2 software. Energy minimization and molecular dynamics methods were combined with the Discover program using a PCFF force field. The structures were minimized with a conjugated gradient method and subjected to a 50 ps dynamics run at 298 K with a 1 fs time step. The radius of gyration for the PEO2k and aliphatic chain lengths for Pyr-C16 and Calix2 were estimated. The alkyl chains in Calix2 were assumed to have an all-*trans* chain conformation due to the confinement to the gold surface. For the PEO2k chain, the hydrodynamic radius was estimated using the obtained radius of gyration assuming a monodisperse random coil in a good solvent.²¹ The obtained data were used only for a rough comparison with the experimental data.

Methodological aspects of dynamic light scattering (DLS) can be found elsewhere.^{22,23} DLS measurements were conducted using a Brookhaven Instruments BI-200SM goniometer, a BIC-TurboCorr digital pseudo-cross-correlator, and a BI-CrossCorr detector, including two BIC-DS1 detectors. Pseudo-cross-correlation functions of the scattered light intensity were collected at 90° scattering angle with the self-beating scheme. A BIC Mini-L30 diode laser operating at the wavelength of $\lambda_0 = 637$ nm and the power of 30 mW was used as a light source. DLS studies were performed at 20 °C. For each sample, 4–5 correlation functions recorded during 40 min were averaged and then analyzed with an inverse Laplace transform program CONTIN.

Results and discussion

Calixarenes with aliphatic thiols attached to two of the four hydroxyl groups were synthesised. Disubstituted calixarene was preferred over a tetrasubstituted one because the previous work by Gutsche and Bauer indicates that unsubstituted OH-

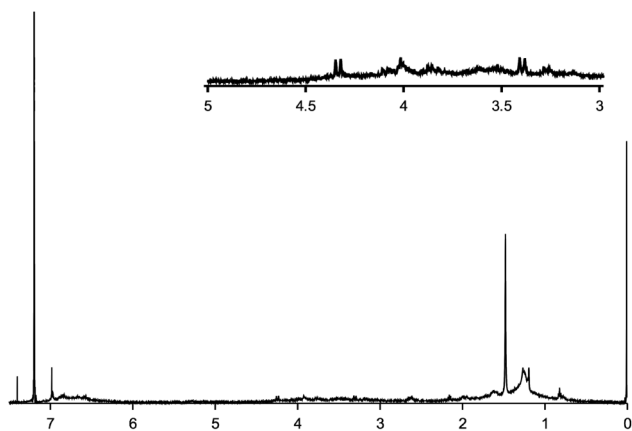


Fig. 4 ¹H NMR spectrum of the purified C-AuNPs. Inset shows region 5–3 ppm in more detail.

groups play a significant role in the complexation behavior.²⁴ It is known that free OH-groups improve the complexation ability the calixarenes.

Calixarene protected gold nanoparticles were synthesised and characterized with thermogravimetric analysis, NMR studies and transmission electron microscopy. The complexation of the nanoparticles with pyridinium compounds were studied with ¹H NMR and light scattering techniques. In this manuscript we denote the resulting products as calixarene only (C-AuNP), calixarene/dodecanethiol (C/D-AuNP) and calixarene/butanethiol (C/B-AuNP) protected nanoparticles.

TGA measurements are shown in Fig. 5, where it can be seen that the thermolysis weight losses were found to be 26.5%, 25.6% and 24.6% (± 0.33) for C-AuNP, C/D-AuNP and C/B-AuNP, respectively. The reaction time for the alkanethiol addition was only 1 hour and the mass loss difference between the nanoparticles is low. However, the small decreasing trend from C-AuNP to C/B-AuNP suggests that at least some ligand exchange has taken place. Because the mass loss differences are very small (less than 2% at the most), the ligand exchange effect to the complexation ability is most likely to be also low. Therefore the alkanethiol modified particles can effectively be considered as C-AuNPs, but with small amounts of ligand exchanged butanethiol or dodecanethiol added to the surface. The effect of the minor ligand exchange is considered further in the later sections.

A representative TEM image is shown in Fig. 6, with size distributions of the different samples. Particles were reasonably monodisperse, with diameters varying between 1.5 and 4.5 nm. The mean diameter was 3.06, 3.10 and 3.11 nm (± 0.7) for C/D-AuNP, C/B-AuNP and C-AuNP, respectively. The result shows that alkanethiol addition had no significant effect on the particle sizes within the experimental error. The size distributions also seem to be almost identical.

For the NMR characterization studies, iodine was used to detach the ligands from the nanoparticles, and integration of the overlapping calixarene/alkanethiol $-\text{CH}_2-\text{S}$ and calixarene aromatic proton signals showed that the molar composition was 13% of butanethiol and 10% of dodecanethiol in C/B-AuNP and C/D-AuNPs, respectively. Using TEM, TGA and NMR data, full characterization of the nanoparticle composition was conducted: the average C-AuNP, C/B-AuNP and C/D-AuNPs

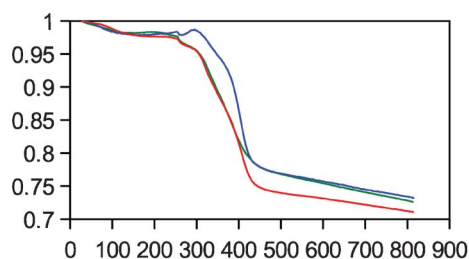


Fig. 5 TGA data for the synthesised nanoparticles, C-AuNP (red), C/B-AuNP (blue) and C/D-AuNP (green).

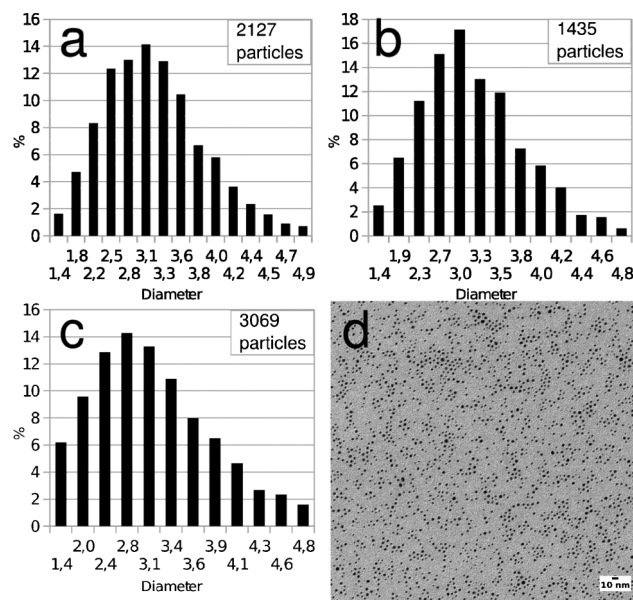


Fig. 6 Transmission electron microscopy size distribution analysis. The number of particles included in the size determination is shown in each distribution graph. a) C-AuNP, b) C/B-AuNP and c) C/D-AuNP. d) A microscopy image of C-AuNP.

were identified as Calix₅₇Au₆₃₅, Calix₅₀Bt₇Au₆₂₉ and Calix₅₀Dod₆Au₆₀₄ nanoparticles.

More detailed data for the nanoparticles is shown in Table 1. Data for previously²⁵ prepared dodecanethiol protected nanoparticles (Dod-AuNP) synthesised in a similar fashion is shown for comparison. The dodecanethiol footprint size is in line with the literature data (21 Å²).²⁶ The area of the calix[4]arene cavity is known²⁷ to be 27 Å². The Calix2 ligands on the C-AuNP surface exhibit roughly a 2.2 times larger footprint area than dodecanethiol protected Dod-AuNPs. The Calix2 footprint area on the NP surface is also 1.7 times larger than the calixarene cavity area. This indicates that the Calix2 aliphatic chains spread away from each other and from the calixarene ring due to steric effects and that the gold surface is much less densely packed with thiolates in the case of Calix2 than in the dodecanethiol case.

As shown by NMR and TGA sections, some ligand exchange has occurred, a small number of calixarenes have been removed and replaced with alkanethiols. The extent of the exchange is, however, so low that any effect on the complexation experiments remain negligible.

During the NMR complexation studies, the NMR signals of calixarene bound onto the nanoparticle surface were broadened due to the motional restriction of the molecules on the surface. However, as seen from the NMR (Fig. 4), there are two obvious doublet signals at 4.4 and 3.4 ppm. These correspond to the methylene bridges between the aromatic rings. It is well known that the symmetry of these signals is broken upon the loss of the cone conformation.³ The symmetrical splitting is clear evidence that the calixarenes attached to the nanoparticles are indeed in the cone conformation.

Table 1 Nanoparticle data. Diameter, gold atoms per cluster, the number of ligand molecules (L) per gold nanoparticle

NP	Diam. (nm)	Au (cluster)	L (cluster)	L (nm ²)	LF (Å ²)
C-AuNP	3.11	635	57	2.18	45.8
C/B-AuNP	3.10	629	50 + 7 ^a	2.23	44.9
C/D-AuNP	3.06	605	50 + 6 ^b	2.22	45.1
Dod-AuNP ^c	3.00	570	110	4.55	22.0

^a Calixarenes + butanethiol. ^b Calixarenes + dodecanethiol, L per nm² and ligand molecule footprint (LF) in Å². All the results were calculated using TGA, NMR and TEM data. Truncated octahedron morphology (circumradius fit for the Archimedean solid and nanoparticle radius observed with TEM) and gold number density of 59 nm⁻³ were assumed^{28,29} in the calculations. ^c Ref 25.

Complexation experiments were performed by mixing different complexants (Pyr-PEO2k-Pyr and Pyr-C16) first with free unbound calixarene and then with calixarene bound on nanoparticles (C-AuNP, C/B-AuNP and C/D-AuNP). In each experiment, pyridinium proton signals shifted from the position characteristic for the pure complexant as the calixarene : complexant ratio was increased. The various host-guest pairs are summarized in Table 2. As an example, Fig. 7 shows the NMR spectra for C-AuNPs mixed with varying amount of Pyr-C16. A significant change in the chemical shift of pyridinium was observed. The change is most considerable for the γ -signal and smallest for the α -signals. The observed changes show the orientation of the pyridinium group in the complex; the γ -proton is deepest inside the calixarene cavity and thus experiences the most significant alteration in its electronic environment.¹⁰

The peak multiplets also show interesting changes; at low calixarene : complexant ratios, the multiplets are clearly visible, but with increasing the ratio the multiplets disappear due to peak broadening. The broadening is attributed to the interaction of the complexant with the calixarene that has been attached to a gold nanoparticle, *i.e.* the motion of the pyridinium is restricted by the complexation.³⁰

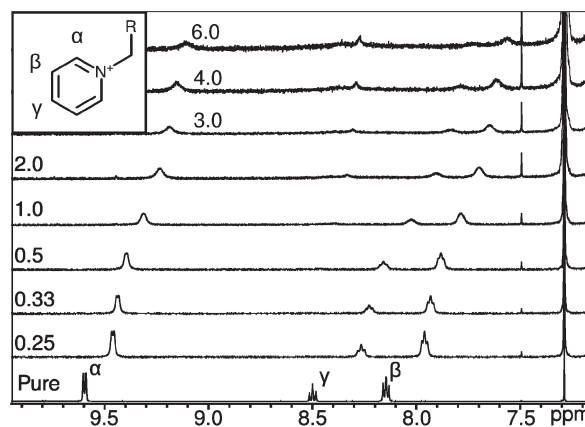
Fig. 8 summarizes the changes in the chemical shifts for all samples. Fig. 8a shows full calixarene : complexant ratio range

Table 2 Complexation result summary for the hosts and guests used.

Broadening: the host : guest ratio range in which the multiplicity broadening occurs. Pure calixarene was omitted due to no bulky gold nanoparticles being present. CCR: calculated complexation ratio (calixarenes per complexant), from the change of the slopes seen in Fig. 8. TCR: theoretical complexation ratio assuming that all the calixarenes present would be fully complexed. C% actual complexation percentage

Host	Guest	Broadening	CCR	TCR	C%
Free calixarene	Pyr-C16	— ^a	0.66	1	66
Free calixarene	Pyr-PEO2k-Pyr	— ^a	0.62	2	31
C-AuNP	Pyr-C16	0.5–1.0	0.69	1	69
C-AuNP	Pyr-PEO2k-Pyr	0.5–1.0	0.72	2	36
C/B AuNP	Pyr-PEO2k-Pyr	0.5–1.0	0.74	2	37
C/D AuNP	Pyr-PEO2k-Pyr	0.5–1.0	0.58	2	29

^a Not determined.

**Fig. 7** NMR proton spectra for C-AuNP/Pyr-C16 complexes. From bottom up: pure complexant and mixtures with an increasing calixarene : complexant ratio.

only for α -protons. For this sample, the β - and γ -proton signals changed so strongly that they overlapped with other signals and were therefore not reliably observable. As seen in Fig. 7, the complexed pyridinium signals are not separate from the free pyridinium signals, which indicates a dynamic guest-host equilibrium between the free and bound pyridinium. Observing the peak position change as a function of host : guest ratio enables the determination of a saturation point. Once host cavities have been saturated, the observed complex signals should move more rapidly towards the free guest signal position upon further addition of free guest. This is shown schematically in Fig. 9. In Fig. 8 the calixarene : complexant ratio where the slope changes was taken as the saturation ratio and the results are summarized in Table 2. Generally, the ppm shift is always stronger for Pyr-C16 than for Pyr-PEO2k-Pyr. This is rationalized by the steric inhibition of pyridiniums and calixarene cavities by the larger polymer coil. Calixarenes bound to NPs exhibit lower shifts than their free calixarene counterparts, which is due to the close proximity of the calixarene rings on the metal surface in the NP case; one guest complexed by a cavity inhibits the complexation of other guests into the neighbouring cavities. For the PEO2k with pyridinium groups at both ends, the complexation ratio is roughly half of the corresponding Pyr-C16 experiment. This is attributed to the relatively low concentration ($C_{\text{tot}} \sim 5 \text{ mg ml}^{-1}$) of the studied system (low amount of complexation induced aggregation of nanoparticles), the random coiling of the polymer (pyridinium hidden inside the coil), and polymer's larger steric blockade of the neighbouring calixarene cavities. Interestingly, the host : guest ratio in which the multiplicity broadening occurs, coincides with the calculated saturation ratio. This supports the validity of the measurements, that at low calixarene : complexant ratios the population of free complexant compounds is high and thus contributes to the visibility of the signal multiplicities. At a high host : guest ratio, most of the pyridiniums are complexed, which suppresses the multiplets due to the broadening that occurs to compounds bound to a stationary surface. The

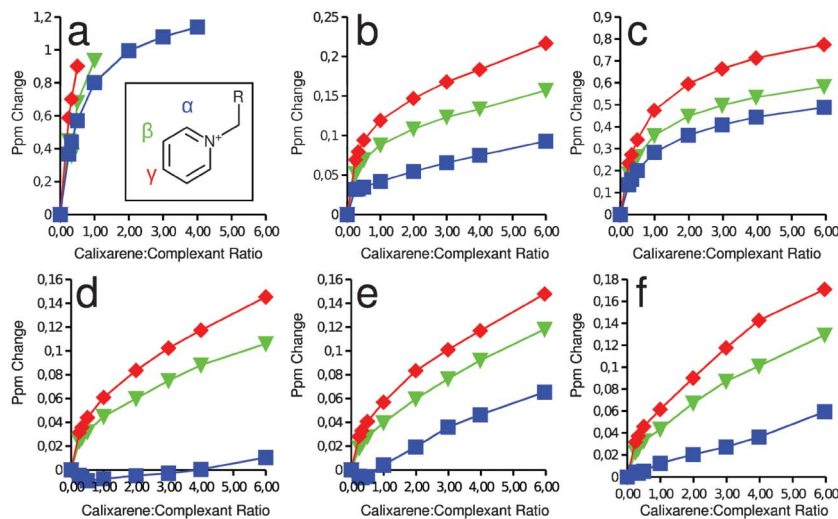


Fig. 8 Calixarene induced change in the pyridinium proton signals compared to the corresponding pure complexant signal position. a) Free calixarene : Pyr-C16; b) free calixarene : Pyr-PEO2k-Pyr; c) C-AuNP : Pyr-C16; d) C-AuNP : Pyr-PEO2k-Pyr; e) C/B-AuNP : Pyr-PEO2k-Pyr; f) C/D-AuNP : Pyr-PEO2k-Pyr. Blue squares, green triangles and red diamonds denote α -, β - and γ -protons, respectively.

broadening range for the free calixarene complexation is not shown in Table 2 because there is no gold nanoparticle to induce the broadening.

According to Table 1 and 2, for C-AuNP and Pyr-C16, on average, 68% of the cavities of a single particle are filled at the saturation host : guest ratio. For C-AuNP and Pyr-PEO2k-Pyr, the corresponding scenario is 37%. The results also show that the calculated complexation ratio is almost the same for both C-AuNP and C/B-AuNP. This clearly shows that the addition of butanethiol on the nanoparticles has a negligible effect on the complexation ability of the nanoparticles. In contrast, the C/D-AuNP complexation ratio is lower than the C-AuNP. Therefore, addition of longer chain dodecanethiol has a detrimental effect on the complexation ability. A likely cause is that the long aliphatic chain inhibits complexation sterically, *i.e.*, the pyridinium cation cannot fully reach the electron-rich ring due to nearby long alkanethiol chains. This suggests that the addition of alkanethiols of varying chain length can be used to fine-tune the sensitivity of metal surface-bound calixarenes. C/D-AuNP and C/B-AuNP showed a similar extent of ligand exchange upon alkanethiol addition, as discussed in the TGA and NMR sections. Since C-AuNP (no alkanethiol) and C/B-AuNP (butanethiol added) have almost identical complexation ratios, the observed ligand exchange effect does not significantly affect the complexation ability.

NMR experiments also provided details on the changes in the chemical environment in the calixarene ring itself. Fig. 10 shows the aromatic region of the free calix[4]arene when complexed with Pyr-PEO2k-Pyr. The effects were observable for all complexants, but barely visible for calixarenes bound to metal nanoparticles. Interesting opposing effects are observed for aromatic protons upon the guest addition. Signals from the aromatics with hydroxyl substituents show a downfield change, which is attributed to the positively charged pyridinium ring interacting with the relatively electron rich

(enhanced resonance stabilization) hydroxyl substituted aromatic ring. The proximity of the pyridinium moiety causes significant but opposite changes in the ether substituted aromatics. The data suggest that the calixarene cavity changes its shape upon complexation. This observation is in line with the previously detected induced fit behavior for calix[8]arenes,¹⁴ and suggests that even the smallest of the calixarene family, calix[4]arene, bound to a nanoparticle surface can undergo an induced fit complexation.

Estimation of dimensions of the compounds indicated that Calix2 is ~ 1.7 nm in length. When attached to the gold core of 1.55 nm radius, the radius for the whole protected nanoparticle was ~ 3.2 nm. The Pyr-C16 chain length was estimated to be 2.0 nm and the R_h for the PEO2k chain was estimated to be ~ 4.6 nm. Assuming a full and dense complexation layer on the nanoparticle calixarene cavities, the expected radii would be ~ 3.3 , ~ 5.3 and ~ 12.5 nm for C-AuNP, C-AuNP + Pyr-C16 and C-AuNP + Pyr-PEO2k-Pyr cases, respectively. Here we do not take into account the case where nanoparticles aggregate *via* complexation.

Light scattering studies were performed in order to estimate the size of the calixarene protected gold particles in chloroform and to investigate possible effects of the pyridinium compounds on their sizes and size distributions. Solutions studied by other techniques in this work were dark red due to the light absorption, practically within the whole range of the visible light spectrum. For LS studies, nanoparticle samples were diluted with chloroform down to 0.2 mg ml⁻¹ and a red laser ($\lambda_0 = 637$) was used to minimize the absorption effect. The studies were performed for samples with a Calix2 : complexant ratio of 0.25, to ensure maximal calixarene cavity saturation.

Fig. 11 shows the distributions of the hydrodynamic radii (R_h). C-AuNP (Fig. 11a) shows particles with R_h ranging from 2 to 20 nm with a mean of 7.6 nm. This suggests that in low

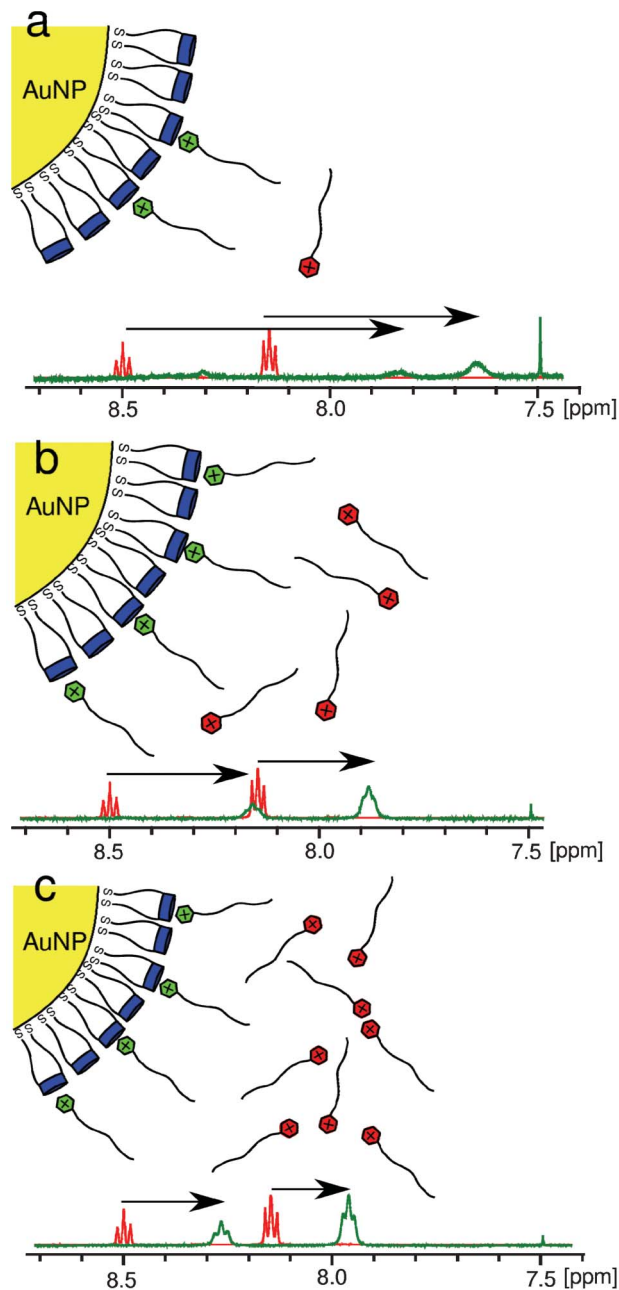


Fig. 9 NMR spectra of the complexes (green) and free Pyr-C16 complexant (red). a) At a high calixarene : complexant ratio (4.0) most of the Pyr-C16 is complexed with the calixarene cavities. Signals from the complexed pyridinium are broadened. b) Until the saturation calixarene : complexant ratio (0.5–1.0), the population of free complexants increases together with the bound complexant. At the saturation point the signal broadening is overcome by the emerging sharp multiplets of the free complexants. c) After passing the saturation ratio towards low (0.25) calixarene : complexant ratios, further addition of complexant increases only the free complexant population. Signals move closer to those of the free complexant and clear sharp multiplets of the free Pyr-C16 become more discernible.

concentrations, C-AuNP can undergo minor aggregation. The distributions shown in Fig. 11 are intensity weighted and the relative contribution of the larger species to the overall

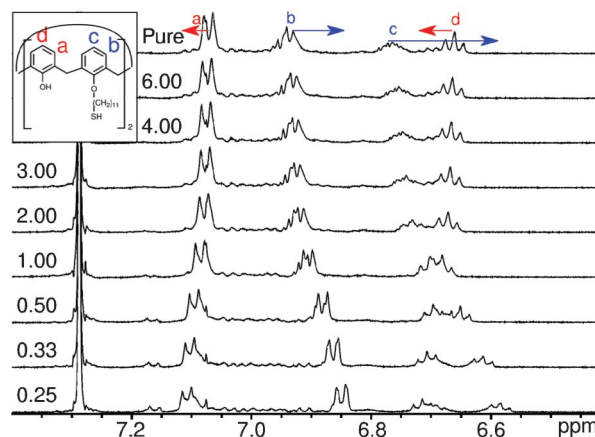


Fig. 10 Calixarene aromatic region for free Calix2 when complexed with Pyr-PEO2k-Pyr. From top to bottom, pure free Calix2 and decreasing Calix2 : Pyr-PEO2k-Pyr ratio. Arrows show how the signal positions change with increasing amount of complexant.

intensity overcomes the contribution of smaller but more numerous scatterers.

Upon addition of Pyr-C16 or Pyr-PEO2k-Pyr, a drastic increase in the particle size is observed. The upper limit of the R_h distribution range increases up to 400 nm and 110 nm for Pyr-C16 and Pyr-PEO2k-Pyr, respectively. A significant portion of the observed scatterers are still of a similar size to the C-AuNP sample, but larger scatterers emerge in addition. The observed R_h is significantly larger than would be expected from the size estimation for individual particles in dispersions of low concentration: the broad distribution indicates the presence of larger aggregates, formed by coupling of several nanoparticles. These aggregates are also visible in the UV-Vis spectra as a slight red shift in the surface plasmon resonance (SPR) band, Fig. 12. NMR complexation results combined with the observed emergence of the larger scatterers suggest that upon Pyr-PEO2k-Pyr addition (Fig. 11c), the nanoparticles are

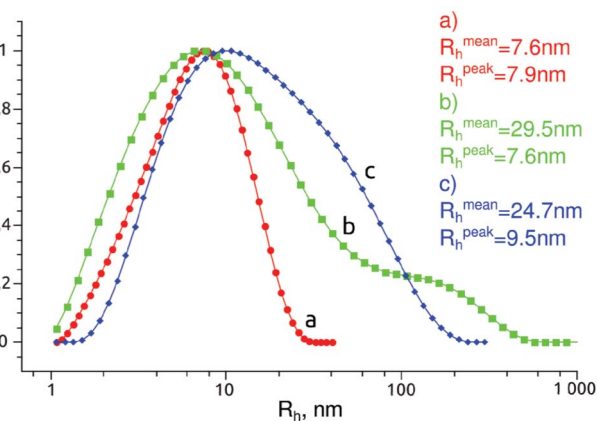


Fig. 11 Distribution of the hydrodynamic radii (R_h): a) C-AuNPs, b) C-AuNP with Pyr-C16 and c) C-AuNP with Pyr-PEO2k-Pyr. Mean and peak values of R_h are shown in the inset.

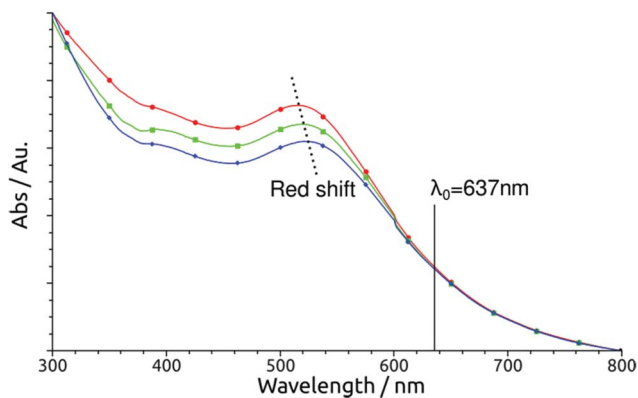


Fig. 12 UV-Vis spectra. From top to bottom: C-AuNPs (red), C-AuNPs + Pyr-C16 (green), CnAuNPs + Pyr-PEO2k-Pyr (blue). SPR absorption maximas are 516, 518 and 522 nm, respectively. $\lambda_0 = 637$ nm, the incident light used in the LS experiments.

linked together with bifunctional polymers. Interestingly, Pyr-C16 addition (Fig. 11b) shows an even larger dispersity shoulder in the size distribution. The expected result would be individual nanoparticles coated with Pyr-C16, because the compound has only one pyridinium moiety. In this case, a similar size distribution, but of a slightly larger size, as for the pure C-AuNP sample would be observed. Obviously this is not the case, and the nanoparticles are clearly aggregated by the action of Pyr-C16.

Interdigitation is a phenomenon that is observed when alkanethiol-protected nanoparticles are dried or cast into a film, first observed by Terrill *et al.*³¹ Interdigitation is also known to occur in solution when the nanoparticle alkanethiol shell is penetrated by an aliphatic chain with a polar group at the end.³² This description is analogous with the Pyr-C16 complexant. Therefore, the observed aggregation upon the Pyr-C16 addition is attributed to the interdigitation of the added pyridinium aliphatic chains into the gold nanoparticle protective shell, forming a secondary monolayer, which facilitates the aggregation due to the propensity of the pyridinium moieties to interact with a calixarene cavity of a neighbouring metal nanoparticle. Interdigitation could be

possible with other complexed pyridinium aliphatic chains or into the protecting calixarene shell itself due to the strong curvature of the surface. For the Pyr-PEO2k-Pyr complexant, the particles are aggregated by mediating polymer chains. In low concentrations, intra-nanoparticle polymer loops are very probable, but due to the dynamic character of the guest-host complexation, the chains are likely to realign themselves when two particles are in close proximity. Upon higher concentrations, the effect of polymer chain entanglement is expected to become more prominent. The proposed complexation interactions for both Pyr-C16 (a) and Pyr-PEO2k-Pyr (b) are shown as a summary in Fig. 13. Since the solutions were studied at low concentration, the formation of even larger aggregates was not observed, but would be expected in solutions of higher concentrations. A high concentration regime can not be studied by LS, however, and this will be the subject of further studies.

Conclusions

Calixarene protected gold nanoparticles with narrow size distribution and a polymeric complexant Pyr-PEO2k-Pyr were synthesised and characterized. The complexation-induced aggregation of the calix[4]arene and calix[4]arene/alkanethiol protected gold nanoparticles were studied with TEM, TGA, UV-Vis, NMR and LS to yield new quantitative information about the complexation phenomenon and links the complexation of the calixarenes to the aggregation of the nanoparticles.

NMR studies showed a significant shift of the pyridinium signals upon complexant addition, broadening of the complexant signal multiplicities upon saturation calixarene : complexant ratios and evidence of induced fit coupling for calix[4]arene. Plotting of signal shifts against the calixarene:complexant ratio allowed the estimation of the saturation point of the complexant addition. The smaller complexant, Pyr-C16, showed higher complexation ability than polymeric Pyr-PEO2k-Pyr. Also free calixarenes complexed more strongly than their metal bound counterparts.

AuNPs complexed with calixarenes were quickly treated with alkanethiols. Just minute amounts of aliphatic com-

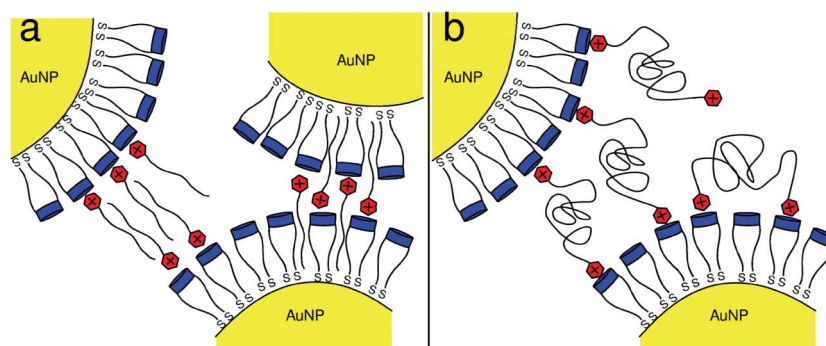


Fig. 13 Proposed aggregation of C-AuNP via complexation of a) Pyr-C16 or b) Pyr-PEO2k-Pyr with the calixarene cavity.

pounds bind to the particle surfaces and a small amount of ligand exchange occurs but that has no significant effect on the complexation ability. Addition of short alkanethiol (butanethiol) among the calixarenes on the gold surface showed no impact on the complexation ability, but the longer dodecanethiol clearly interfered with it, suggesting the possibility of tuning the calixarene complexation ability or selectivity.

Light scattering experiments, combined with TGA and TEM, showed interesting results for C-AuNP nanoparticles. In the TEM images, the average diameter of C-AuNP was found to be 3.11 nm, with ~60 calixarene groups attached per gold nanoparticle. Complexation studies showed that at the saturation ratio, Pyr-C16 pyridinium groups, on average, complexed with 69% of these cavities. For polymeric Pyr-PEO2k-Pyr the corresponding value was 36%. Light scattering studies, confirmed with UV-Vis spectroscopy, showed that addition of Pyr-PEO2k-Pyr induced the aggregation of the particles. However, even larger aggregates were formed when C-AuNP was complexed with Pyr-C16. This was rationalized by assuming solution phase interdigitation of polar Pyr-C16 molecules, either into metal nanoparticle bound calixarene shell itself or other Pyr-C16 aliphatic chains attached to the electron rich calixarene cavity.

Acknowledgements

We would like to thank the FUNMAT Center of Excellence for Functional Materials and the Academy of Finland (project no. 127329) for financial support. We also thank Janne Ruokolainen and Jani Seitsonen for assistance with TEM measurements. Sami Hietala is thanked for assistance with the Material Studio software.

References

- M. Brust, M. Walker, D. Bethell, D. J. Schiffrin and R. Whyman, *J. Chem. Soc., Chem. Commun.*, 1994, 801–802.
- G. Ozin and A. Arsenault, *Nanochemistry: A chemical approach to nanomaterials*, Royal Society of Chemistry, Cambridge, 2005, pp. 265–319.
- C. D. Gutsche, *Calixarenes*, Royal Society of Chemistry, Cambridge, 1989, pp.149–181.
- M.-C. Daniel and D. Astruc, *Chem. Rev.*, 2004, **104**, 293–346.
- A. Wei, *Chem. Commun.*, 2006, 1581–1591.
- J.-M. Ha, A. Solovyov and A. Katz, *Langmuir*, 2009, **25**, 10548–10553.
- C. Han, L. Zeng, H. Li and G. Xie, *Sens. Actuators, B*, 2009, **137**, 704–709.
- A. Arduini, D. Demuru, A. Pochini and A. Secchi, *Chem. Commun.*, 2005, 645–647.
- F. Ciesa, A. Plech, C. Mattioli, L. Pescatori, A. Arduini, A. Pochini, F. Rossi and A. Secchi, *J. Phys. Chem. C*, 2010, **114**, 13601–13607.
- S. Ishihara and S. Takeoka, *Tetrahedron Lett.*, 2006, **47**, 181–184.
- M. Dionisio, F. Maffei, E. Rampazzo, L. Prodi, A. Pucci, G. Ruggeri and E. Dalcanale, *Chem. Commun.*, 2011, **47**, 6596–6598.
- J.-M. Ha, A. Katz, A. B. Drapailo and V. I. Kalchenko, *J. Phys. Chem. C*, 2009, **113**, 1137–1142.
- J.-M. Ha, A. Solovyov and A. Katz, *Langmuir*, 2009, **25**, 153–158.
- J.-M. Ha, A. Solovyov and A. Katz, *J. Phys. Chem. C*, 2010, **114**, 16060–16070.
- C. D. Gutsche and M. Iqbal, *Org. Synth.*, 1989, **68**, 234–236.
- R. Métivier, I. Leray, B. Lebeau and B. Valeur, *J. Mater. Chem.*, 2005, **15**, 2965–2973.
- J. Gong, V. G. Vaidyanathan, X. Yu, T. W. Kensler, L. A. Peterson and S. J. Sturla, *J. Am. Chem. Soc.*, 2007, **129**, 2101–2111.
- M. Brust, D. Bethell, C. J. Kiely and D. J. Schiffrin, *Langmuir*, 1998, **14**, 5425–5429.
- A. C. Templeton, M. J. Hostetler, C. T. Kraft and R. W. Murray, *J. Am. Chem. Soc.*, 1998, **120**, 1906–1911.
- Z. Tang, D. A. Robinson, N. Bokossa, B. Xu, S. Wang and G. Wang, *J. Am. Chem. Soc.*, 2011, **133**, 16037–16044.
- W. Burchard, *Advances in Polymer Science*, Springer Verlag, Berlin Heidelberg, 1999, **vol. 143**, pp. 113–194.
- B. Chu, *Laser Light Scattering: Basic Principles and Practice*, Academic Press, Boston, 1991, pp. 4–318.
- W. Schärtl, *Light Scattering from Polymer Solutions and Nanoparticle Dispersions*, Springer Verlag, Berlin Heidelberg, 2010, pp. 1–183.
- L. J. Bauer and C. D. Gutsche, *J. Am. Chem. Soc.*, 1985, **107**, 6063–6069.
- A. Määttänen, P. Ihalainen, P. Pulkkinen, S. Wang, H. Tenhu and J. Peltonen, *ACS Appl. Mater. Interfaces*, 2012, **4**, 955–964.
- R. G. Shimmin, A. B. Schoch and P. V. Braun, *Langmuir*, 2004, **20**, 5613–5620.
- O. Kuchma, Y. Zub and A. Dabrowski, *Colloid J.*, 2006, **68**, 721–728.
- R. L. Whetten, J. T. Khoury, M. M. Alvarez, S. Murthy, I. Vezmar, Z. L. Wang, P. W. Stephens, C. L. Cleveland, W. D. Luedtke and U. Landman, *Adv. Mater.*, 1996, **8**, 428–433.
- M. K. Corbierre, N. S. Cameron and R. B. Lennox, *Langmuir*, 2004, **20**, 2867–2873.
- M. J. Hostetler, J. E. Wingate, C.-J. Zhong, J. E. Harris, R. W. Vachet, M. R. Clark, J. D. Londono, S. J. Green, J. J. Stokes, G. D. Wignall, G. L. Glish, M. D. Porter, N. D. Evans and R. W. Murray, *Langmuir*, 1998, **14**, 17–30.
- R. H. Terrill, T. A. Postlethwaite, C. Chen, C.-D. Poon, A. Terzis, A. Chen, J. E. Hutchison, M. R. Clark and G. Wignall, *J. Am. Chem. Soc.*, 1995, **117**, 12537–12548.
- A. Swami, A. Kumar and M. Sastry, *Langmuir*, 2003, **19**, 1168–1172.